Automatic interpretation of cod otoliths using deep learning

Endre Moen[1*], Rune Vabø[1], Szymon Smoliński[3], Come Denechaud[1], Ketil Malde[1,2],

1 Institute of Marine Research, Bergen, Norway

2 Department of Informatics, University of Bergen, Norway

3 Department of Fisheries Resources, National Marine Fisheries Research Institute, Kołłataja 1, 81-332 Gdynia, Poland * endre.moen@hi.no

Abstract

Introduction

Knowledge of fish age structure is central to the study of fish and stock dynamics. It informs on population growth and mortality and is one of the main criteria used for determining the health of exploited populations and monitoring the effects of selective fishing (Brunel and Piet, 2013; Hidalgo et al., 2011). Changes in the age distribution can track significant changes in population structure, such as a particularly strong year-class skewing the distribution (Reglero and Mosegaard, 2006), or the gradual truncation of older age classes as selective fishing mortality removes larger individuals (Siskey et al., 2016). Hard structures such as scales and otoliths are used worldwide as one of the primary sources of fish age estimates, due to their ability as natural physiological and environmental recorders to form regular, temporally resolved growth increments at the daily and annual levels (Albuquerque et al., 2019; Campana, 2001; Francis and Campana, 2011). While age is inferred from the “simple” counting of annual increments, the interpretation of this zonation pattern is species or even population-specific (Høie et al., 2009) and is based on precise knowledge of the timing of zone formation and of the correct identification of true and false zones (Panfili et al., 2002). This process therefore requires specific expertise and is subject to uncertainties in both between-reader precision and “true” age accuracy (Francis and Campana, 2011). Therefore, streamlining, scaling, and increasing the quality of age estimations can improve the reliability of evaluations of fish biology and consequently stock size and structure (Beamish and McFarlane, 1995; Ragonese, 2018; Tyler et al., 1989).

Otolith reading is time and resource consuming. Training of expert readers can take several years depending on the species, and otoliths often undergo a long processing phase before the final age estimates can be produced (Carbonara and Follesa, 2019). This is particularly true for demersal fish species, like Atlantic cod (Gadus morhua), that have large opaque otoliths that typically require time-consuming preparation. These routines vary between populations and institutes and range from direct reading of broken otoliths under a magnifying glass, to embedding, thin sectioning and finally imaging of the sections under a microscope. There has been a variety of methods proposed to automatically interpret otoliths, which range from one-dimensional data analysis like intensity transects (Mahé, 2009) to the more recent effort toward developing machine learning (ML) frameworks (Moen et al., 2018; Politikos et al., 2021).

About deep learning and image analysis

Deep learning has during the last decade become the dominating field of machine learning where various architectures of deep neural networks are able to learn to efficiently identify patterns and structures in various types of data (LeCun et al., 2015)(LeCun, 2015). Within computer vision, deep Convolutional Neural Networks (CNN) have been prevailing the field ever since Krizhevsky et al. in 2012 (Krizhevsky et al., 2012)(Krizhevsky et al., 2012) won the annual ImageNet Large Scale Visual Recognition Challenge (ILSVRC) competition (Russakovsky et al., 2014)(Russakovsky et al., 2015). CNNs have seen a continuous development with new improved architectures arising year by year. ILSVRC remains the most important benchmark for image classification, with 1.4 million images in the ImageNet training set. The state-of-the-art CNNs are therefore heavily trained on a lot of images. Many of these CNNs are publicly available including their trained network weights. This enables the use of transfer learning from one image domain to another providing a very useful pre-trained starting point for further training of more specific image classification tasks were much less images are available. Age estimation from images of otoliths represents, for several fish species, precisely such a task. InceptionV3 (Szegedy et al., 2015) was modified to predict the age of Greenland halibut (Reinhardtius hippoglossoides) from otolith images (Moen et al., 2018), and a modified InceptionV3 was applied to classify otolith images of red mullet (Mullus barbatus) (Politikos et al., 2021). While some state-of-the-art CNNs grew in model size a recent CNN architecture called EfficientNet (Tan and Le, 2019)(Tan and Quoc, 2019) demonstrated that increased performance could be achieved with smaller model sizes (number of parameters) using a compound scaling method for network depth, width and image size, resulting in a family of seven different models with different sizes. This network has been successfully applied with transfer learning to analyse images of salmon scales (Vabø et al., 2021)(Vabø et al., 2021). Recently an even more compute efficient family of model architecture is called EfficientNetV2 (Mingxing Tan and, 2021) has become part of the state-of-the-art CNNs and has been made available.

In this study, we develop a learning framework for automating the age estimation of Atlantic cod based on multi-exposure images of broken otoliths. We apply the two EfficientNet family architectures EfficientNetV1 and EfficientNetV2 using three and two different model sizes from each family respectively. We compare the performance of the different models and discuss the use of ensemble of models to improve estimation accuracy.

Method and materials

Data Collection

We used a data set sampled from 5150 cod otoliths which was collected on surveys in the period 2012-2018 conducted by Institute of Marine Research (IMR) and aged by otolith experts. On each of the surveys, the otoliths were sampled using a random-stratified sampling based on fish length for each trawl station, and the otoliths from individual fish were randomly sampled.

The details of how the data-set was collected and sampled from surveys, camera and mount setup, how the otolith was processed before imaging, the resulting exposures, and naming and folders organization can be found in (et al. et al., 2019) as well as where the data-set is available (https://doi.org/10.21335/NMDC-1826273218).

The otolith was broken in the transverse plane and placed on a mount, before it was captured by six images with three light exposures and one rotation of 180°. We used the first 3 images, which positioned the otolith so the proximal surface was close to the top of the image. Figure 1 shows an example of the six image exposures taken of an otolith.

Figure 1. Otolith from 2016 with read age 6 years and light exposure medium, low, and high, then rotated 180° and three new images.

The images were taken with a resolution of 3744×5616 pixels. The image light exposure varied depending on light condition outside, and was stored in the metadata of the JPG file. Typically the exposure order was middle-dark-light, then the rotation, and then middle-light-dark again, but the order could vary. The exact order was recovered by reading the 'ExposureTime' metadata property.

Figure 2 shows the age distribution of the 5150 otoliths in the data set, and figure 3 shows the age distribution selected at random from the data set as the test set consisting of 10% of the whole data set (515 otoliths).

Convolutional neural network architecture

Table 1. EfficientNet and EfficientNetV2 models trained with image exposure. The models are numbered for reference of chapter on ensembles later

CNN family /	EfficientNet			EfficientNetV2	
Image exposure	B4	B5	B6	Medium	Large
Minimum	1	2	3	4	5
Medium	6	7	8	9	10
Maximum	11	12	13	14	15
All (3 images)	-	-	-	16	17

Each CNN was trained using transfer learning by loading ImageNet weights. The images were resized from 3744×5616 pixels to between 380×380 and 528×528 pixels

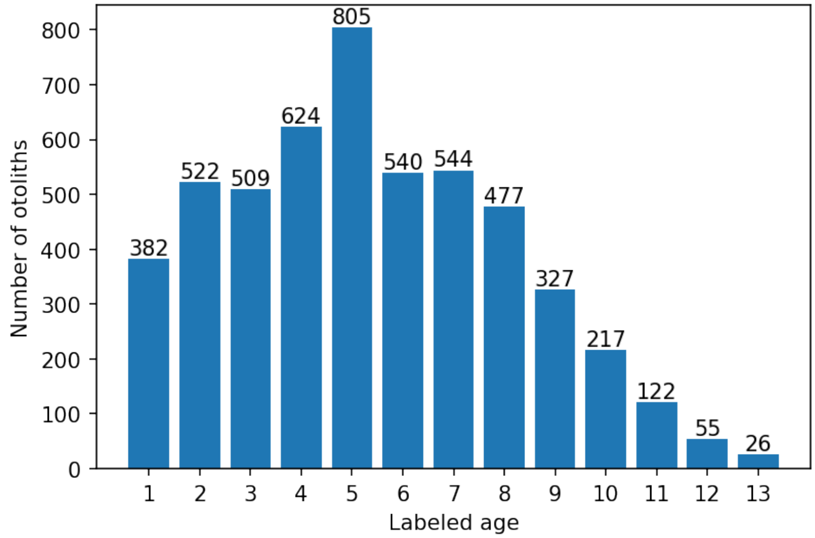

Figure 2. Age distribution of all 5150 images

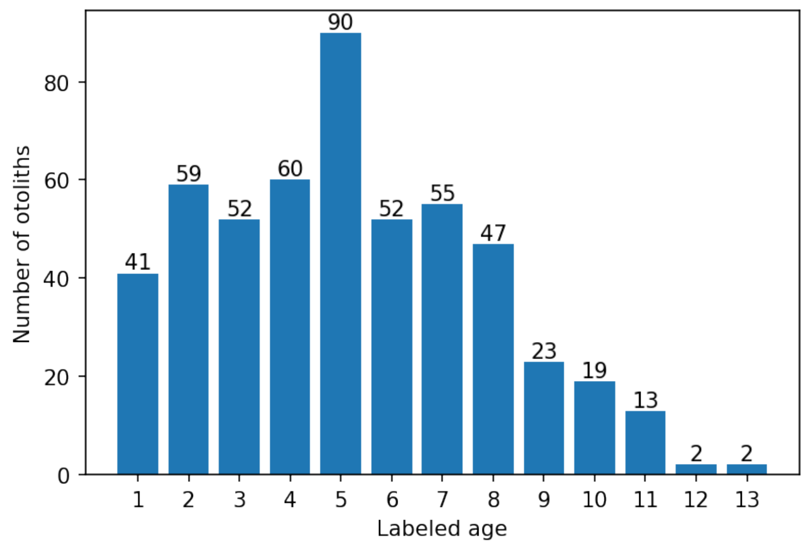

Figure 3. Age distribution of 515 images from the test set

depending on the architecture. The pixel values have a range between 0 and 255, which was normalized to between 0 and 1. While test set size prediction was done on 380×380 and 384×384 pixels. To investigate the image-taking protocol described in (et al. et al., 2019) we also trained on 9-channel images by stacking 3 RGB images representing 3 different lighting exposures. Using Timm(Wightman, 2019), the imageNet weights were duplicated on the input layer to accommodate 9 channels. The three images used were of dark, medium and light exposure of the first orientation. Figure 4 shows an example of the 4 exposures used for training and testing the models.

Figure 4. Otolith from 2013, read age: 6 years, and with light exposure: medium, low, high, and expectation per channel of the three exposures (9-channels).

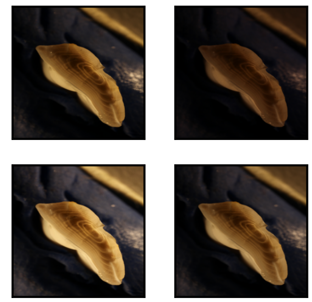

CNNs were selected based on performance on the ImageNet benchmark and availability of open-source implementations with imageNet weights. The imageNet benchmark is for classification while we treated aging as a regression problem (Moen et al., 2018) (Vabø et al., 2021). The last layer of the CNNs was modified to output a linear output. In the EfficientNetV2 family we did this by applying three multi-layer perceptron layers going from 1280 output of the last hidden layer to a dense 256-layer, then a leakyRelu (Xu et al., 2015) layer, then a dense 32-layer, then a leakyRelu layer, and finally a linear output layer. For EfficientNet we only changed the last layer from softmax output to a linear output.

To each fold we normalized the age on the training-set by subtract the mean and scaling to unit variance. The normalization was then applied to the validation and test set. Test set predictions were obtained by applying the inverse transform.

Implementation and training

EfficientNetV1 B4, B5, and B6 were imported and modified with TensorFlow (Abadi et al., 2016) and Keras (Chollet and others, 2018) software packages in Python. Computation was done using CUDA 11.1 and CuDNN with Nvidia(Nvidia Corp., Santa Clara, California) A6000 accelerator card with 48 GB of GPU memory and P100 cards with 12 GB of GPU memory, EfficientNetV2 Medium, and Large were imported and modified with the PyTorch (Paszke et al., 2019) and Timm (Wightman, 2019) software packages. Computation was done on P100 and RTX 3090 with 24 GB of GPU memory. Pretrained weights for EfficientNet were available from Keras, and pretrained weights for EfficeintNetV2 were available from Timm.

Augmentation was applied to the training-set. The images were augmented using rotation between 0 and 360 degrees, and reflection by the vertical axis.

The cost-function used was mean squared error (MSE) while the metric used for evaluating the models and comparing it to expert readers was accuracy. Accuracy was obtained by rounding the floating point number predictions to nearest integer and comparing the age classification against the true labels.

The dataset of 5150 otoliths were divided into a training set constituting 90% of the otolith images (4635 otoliths) and a test set of 10% (515 otoliths). To get the most out of a small data-set we applied 10-fold cross-validation on the training set. This meant that 10% of the training set were used for validation and 90% (81% of the whole data set) were used for the actual training for each fold. Consequently 10 different models were trained with a different set of 463 images used for validation in each fold, i.e. each data point participates in the validation set once and in the training set 9 times. Among the 10 fold models, the one with the best MSE was chosen. The best model-parameters on the validation set were then used to predict the age on the test-set, and the metric for accuracy and MSE were recorded. The test-set is chosen at random, while the 10-fold split is chosen using stratified-kfold split, which preserves a similar distribution of the whole cross-validation set in each validation set. That means the 463 images in the validation-set will have similar age distribution to that of the 4635 images in the cross-validation set.

Hyper-parameters

The CNN hyper-parameters configurations varied a little between the two families of networks, but were kept the same within the families. Some hyper-parameters that were tuned are batch size, learning rate, k-fold size, weight decay, step size, number of epochs, early stopping, and patience. Some parameters are constrained by the GPU memory, like batch-size which was kept at 8, except for the B6 model, which was run on the A6000 card.

EfficientNet used learning-rate with weight decay scheduler, while EfficientNetV2 used Cosine Annealing scheduler (Loshchilov and Hutter, 2016). The training- and validation image size used was as described in the papers, except for Large which uses smaller validation image size. The exact configuration of each network is available with each network result in the GitHub page of the project (https://github.com/emoen/Deep-learning-for-regression-of-cod-otoliths).

Table 2. Hyper-parameters on each model

Param/CNN	B4	B5	B6	Medium	Large
`train_batch_size`	8	8	16	8	8
`img_size`	380	456	528	384	384
`val_img_size`	380	456	528	384	384
`steps_per_epoch`	1600	1600	1600	1600	1600
`epochs`	150	150	250	450	450
`early_stopping`	-	-	-	40	40
`early_stopping_patience`	14	14	22	-	-
`reduceLROnPlateau_patience`	7	7	11	-	-

Medium all-, and min-exposures was run with `steps_per_epoch`=160
B6 has epochs=150, `early_stopping_patience`=14, and `reduceLROnPlateau_patience`=7
B4 min was run with `img_size`=456

Table 3. Hyper-parameters on all models, TensorFlow only (B4,B5, B6), and PyTorch only (Medium and Large)

`Parameter`	Value	TensorFlow	PyTorch
`learning_rate`	1e-05	v	v
`n_fold`	10	v	v
`test_size`	0.1	v	v
`in_chans`	3 or 9	v	v
`reduceLROnPlateau_factor`	0.2	v	x
`which_exposure`	min, medium, max	v	x
`scheduler`	CosineAnnealingLR	x	v
`T_max`	10	x	v
`min_lr`	1e-06	x	v
`weight_decay`	1e-06	x	v
`which_exposure`	min, medium, max, all	x	v

`in_chans` is the number of channels as input for the model. It was either 3 for an RGB image or 9 channels for 3 images.

Ensemble learning with averaging

Ensemble learning is an algorithm that combines the predictions from multiple models to reach a final prediction, and obtains a predictive performance that is better than any of the constituent models alone.

There are many algorithms that perform ensembles to reach a prediction. E.g. bagging, stacking and boosting ensembles. We use simple ensemble average which is a form of bagging ensemble. Another example of a bagging ensemble is a voting ensemble.

The ensemble average reduces the variance of the prediction and does not change the mean. The reduced variance improves the model performance. An ensemble can make better predictions and achieve better performance than any single contributing model, just as more experts will produce higher accuracy in predicting a single otolith. The ensemble prediction is therefor more robust because it reduces the spread of the predictions and model performance.

We evaluate two types of simple ensemble average. The first ensemble is the average of the 10-fold cross-validation, which was reported as the model performance. This ensemble was reported as the performance of one model but we obtain 10 different models which contains the weights that gave the best MSE on the validation set, and the average of the prediction on the test set was reported as the accuracy after rounding.

The second ensemble was created by combining models where we look at tuple-ensembles, consisting of 2 models, triplets, quadruples and so on, to ensemble of all 17 models which contained 20, 30 and so on up to 170 predictions on the test set. The accuracy was reported after rounding.

By choosing the best model we were over fitting to the test set, but a subset of the best simple ensemble average learners will likely produce a better prediction on a hold-out test set than any of models.

Correlation of predictions on the test set and clustering analysis

We have looked at the correlations of predictions on the test set by creating a correlation matrix of each models prediction of each age class. This showed how much the models were in agreement with each other. Clustering analysis identified which models were more in agreement with each other.

The relations between the model-predictions was linear therefor we used Pearson's correlation coefficient. Clustering analysis on the Pearson's correlation coefficient matrix was done by inspecting hierarchical clustering (HCA), and K-Means clustering with the number of clusters given by the elbow-, and the silhouette-score-method. With HCA we used Euclidean distance (Chebyshev distance, and Minkowski distance gave similar results), and we used Complete-Linkage clustering. The resulting clusters were drawn using a dendrogram. The key to interpreting the dendrogram is to focus on the height at which any two objects are joined together. The lower the height the more similar the two objects are.

Results

The mean accuracy of the 17 models was 72.7% (table 4) on the test-set, and the standard deviation was 1.1. The least accurate model was B4-max, and the most accurate model was B5-min and B6-middle with accuracy of 74.4%. Assuming a normal distribution, the probability of seeing a model with lower accuracy than B4-max is less than 4.8% and the probability of seeing a model with higher accuracy than B5-min or B6-middle is less than 6.5%. The accuracy is not significantly different (p=0.05) between B5-min (or B6-middle) and B4-max model.

B5 was the best model on all the exposures(min, middle, max) with a mean accuracy of 73.7%, and min-exposure was the best exposure with a mean accuracy of 73.3% Both B5 and B6 from the EfficientNet family was better than Medium and Large from the EfficientNetV2 family.

Table 4. Mean accuracy on the test-set by light exposure and CNN architectures

Acc:light/CNN	B4	B5	B6	Medium	Large	Mean
min	72.8*	**74.4**	73.4*	74.0	72.0	73.3
middle	71.5	73.4	**74.4**	72.4	72.8	72.9
max	70.9	73.2	71.5	71.3	72.4	71.9
9 channels	-	-	-	74.0	72.2	73.1
Mean	71.7	73.7	73.1	72.9	72.4	72.7

The mean MSE of the 17 models was 0.284 (table 5) on the test-set, and the standard deviation was 0.022. The highest MSE was from B5-max with MSE of 0.359, and the lowest MSE was from B6-middle exposure with MSE of 0.262. Assuming a normal distribution, then the probability of seeing a model with higher MSE than B6-max is less than 0.03% and the probability of seeing a model with lower MSE than B6-middle is less than 15.7%.

Medium and Large were the best models with a MSE of 0.278, and the all-exposure (9-channel images) was the best exposures with a MSE of 0.272. The high MSE for B5-max and B6-max was due to a large misprediction of image with index 308 in the test-set (see chapter on Outliers).

Figure 5 shows a box-plot of each 10-fold ensemble average prediction on accuracy, and MSE for all the 17 models. The red lines are the ensemble-average predictions with

Table 5. Mean MSE on the test-set by light exposure and CNN architectures

MSE:light/CNN	B4	B5	B6	Medium	Large	Mean
min	.277	.277	.272	.273	.280	.276
middle	.285	.273	**.262**	.278	.275	.275
max	.291	.359	.305	.289	.286	.306
9 channels	-	-	-	.273	.271	.272
Mean	.284	.303	.280	.278	.278	.284

highest accuracy. The blue lines are the other ensemble average predictions. The orange lines are the mean accuracy or MSE. The ensemble metric was either better than or in the upper quantile for all the models. The prediction MSE and accuracy of each fold are given in table 12 and 13 in appendix C.

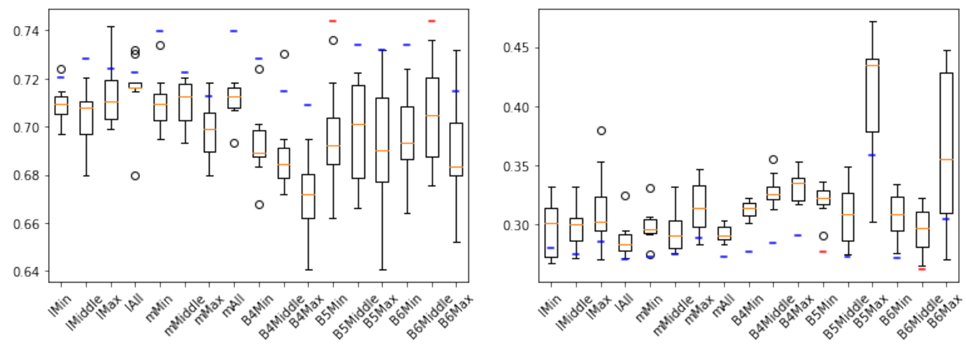

Figure 5. A box-plot of accuracy score (left) and MSE (right) of all the 17 models and the blue line is ensemble-average prediction accuracy (or MSE) on the test-set. The red lines are the two best ensemble-average predictions on accuracy. The orange line are the mean of the 10-fold predictions.

Prediction by age class

When taking the accuracy of all models by age class, we found that accuracy for one- and two-year-old's was better than 90% (figure 6). All age classes six years or younger were correctly classified with more than 70% accuracy, and all 13-year-old's were predicted to be younger (see Figure 15 in appendix B which shows model the mean and standard deviation from the residuals test set prediction by age classes).

No systematic bias in the age prediction of CNN is visible, except for the underestimated age of individuals aged by human reader as 13 year old (figure 7).

Figure 6. Predictions by age class from the average of all models. The green region shows the correctly classified age after rounding. The axis is fixed, hence large outliers will not be visible.

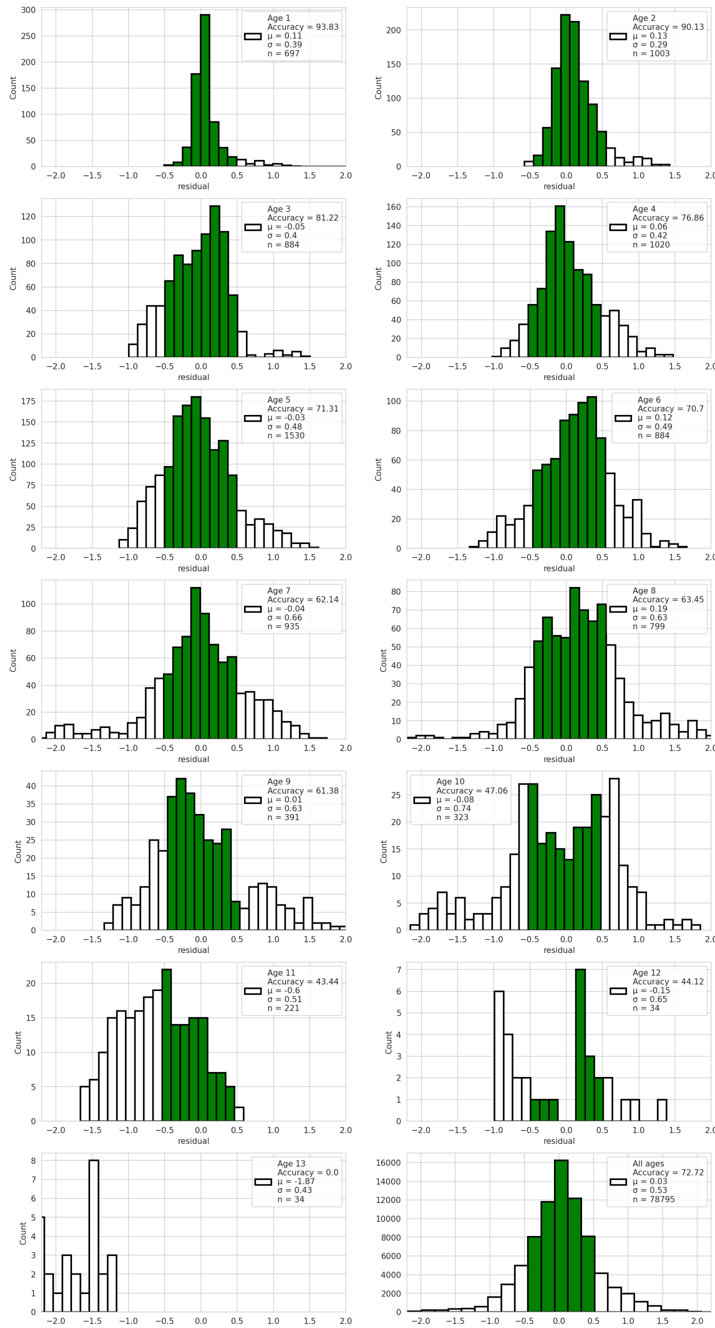

Simple ensemble-average predictions

We searched the space of ensembles-average predictions of 2 to 17 models, which is the set of unordered combinations without replacement, equal to the binomial coefficient

Figure 7. Violin plot of predicted age from model B5-min with accuracy of 74.4%. Above each age is the accuracy, and below is the total number of images in the test set of that age class

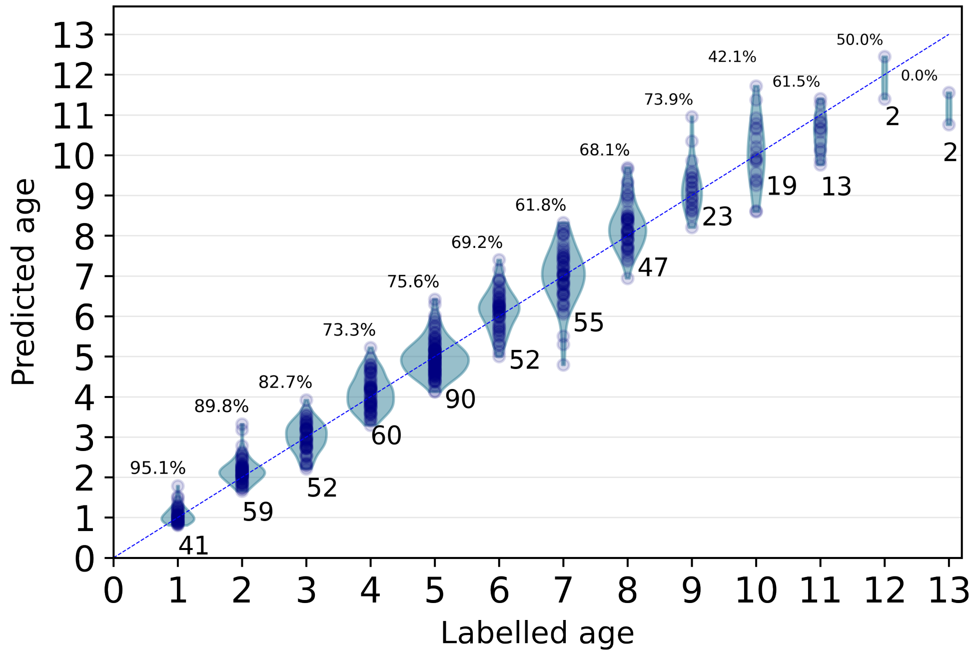

$\sum_{k=1}^{N} \binom{N}{k}$ where $N = 17$ and $k \in 2..N$ For each set of ensemble combination we recorded the best ensemble and found that the best overall ensemble-average prediction was an ensemble of six models which produced an accuracy of 78.6%. The ensemble consisted of B4-min, B5-min, B6-min, Medium-min, B6-middle, and B4-max.

Table 6 shows first the number of combinations of models that exists of tuples, triplets and so on labeled with heading "Coeff", then the best ensemble-average accuracy on the given number of combinations, and then the model-numbers that produced the best combinations. Model-number can be translated to model name using 1. Table 7 shows the same information but selected to minimize MSE.

The ensemble accuracy decreased after adding 6 models, while the MSE continued to decrease until all 17 models were included. This was as expected from the theory on simple ensemble average learning, since the variance is reduced with more models.

We observe that model B4-min (No 1), and B6-min (No 3) were the best models

Table 6. Binomial combinations of simple average of ensembles accuracy

Coeff	#Comb	Best	Mean	Ensemble (see table 1)
2	136	75.9	74.1	(2, 5)
3	680	77.5	74.6	(1, 3, 4)
4	2380	77.9	74.9	(1, 2, 3, 4)
5	6188	77.9	75.1	(1, 2, 3, 4, 11)
6	12376	78.6	75.2	(1, 2, 3, 4, 8, 11)
7	19448	78.1	75.2	(1, 2, 3, 4, 7, 8, 11)
8	24310	77.5	75.2	(1, 2, 3, 4, 7, 8, 10, 11)
9	24310	77.5	75.3	(1, 2, 3, 6, 7, 8, 9, 11, 17)
10	19448	77.1	75.2	(1, 2, 3, 6, 7, 8, 9, 10, 12, 13)
11	12376	76.9	75.2	(1, 2, 3, 4, 6, 7, 8, 10, 11, 13, 16)
12	6188	76.7	75.2	(1, 3, 4, 7, 8, 10, 11, 13, 14, 15, 16, 17)
13	2380	76.3	75.1	(1, 3, 4, 7, 8, 9, 10, 11, 13, 14, 15, 16, 17)
14	680	75.9	75.1	(1, 2, 3, 4, 5, 8, 9, 10, 11, 12, 13, 14, 16, 17)
15	136	75.7	75.0	(1, 2, 3, 4, 5, 7, 8, 9, 10, 12, 13, 14, 15, 16, 17)
16	17	75.5	75.0	(1, 2, 3, 4, 5, 6, 7, 8, 9, 10, 12, 13, 14, 15, 16, 17)
17	1	74.8	74.8	(1, 2, 3, 4, 5, 6, 7, 8, 9, 10, 11, 12, 13, 14, 15, 16, 17)

Table 7. Binomial combinations of simple average of ensembles MSE

Coeff	#comb	best	Mean	Ensemble (see table 1)
2	136	0.250	0.265	(3, 17)
3	680	0.246	0.259	(1, 3, 5)
4	2380	0.245	0.256	(1, 3, 5, 7)
5	6188	0.245	0.254	(1, 3, 4, 7, 17)
6	12376	0.244	0.252	(1, 2, 3, 5, 8, 16)
7	19448	0.244	0.251	(1, 2, 3, 4, 5, 8, 11)
8	24310	0.244	0.251	(1, 2, 3, 4, 5, 8, 11, 17)
9	24310	0.244	0.250	(1, 2, 3, 4, 5, 7, 8, 11, 17)
10	19448	0.244	0.250	(1, 2, 3, 4, 5, 7, 8, 11, 16, 17)
11	12376	0.245	0.250	(1, 2, 3, 4, 5, 7, 8, 10, 11, 13, 16)
12	6188	0.245	0.249	(1, 2, 3, 4, 5, 6, 7, 8, 10, 11, 16, 17)
13	2380	0.245	0.249	(1, 2, 3, 4, 5, 6, 7, 8, 10, 11, 13, 16, 17)
14	680	0.245	0.249	(1, 2, 3, 4, 5, 6, 7, 8, 9, 10, 11, 13, 16, 17)
15	136	0.246	0.249	(1, 2, 3, 4, 5, 6, 7, 8, 9, 10, 11, 13, 15, 16, 17)
16	17	0.247	0.248	(1, 2, 3, 4, 5, 6, 7, 8, 9, 10, 11, 13, 14, 15, 16, 17)
17	1	0.248	0.248	(1, 2, 3, 4, 5, 6, 7, 8, 9, 10, 11, 12, 13, 14, 15, 16, 17)

with inclusion in 14 ensembles(table 8). These models did not have the highest accuracy (B5-min, and B6-middle with 74.6%) but an accuracy of 72.8% and 73.4%. This was lower than the the highest accuracy models, which was B5-min and B6-middle, which had a rank of 3 and 5 respectively.

Exposure-types ranked by how many times they were included in an ensemble was as follows: min-exposure (rank 4.4), middle-exposure (rank 8.6), all-exposures (rank 10), and max-exposure (rank 11.2). EfficientNet had a rank of 6.6 and EfficientNetV2 had a rank of 10.3.

Table 8. Rank of number of times a model is in an ensemble selected by accuracy

Rank	Model name	Count
1	B4_min	15
1	B6_min	15
3	B5_min	13
3	M_min	13
5	B6_mid	12
6	B5_mid	10
6	B4_max	10
8	L_mid	9
9	B6_max	8
10	M_mid	7
10	M_all	7
10	L_all	7
13	M_max	6
14	L_min	5
14	B4_mid	5
14	B5_max	5
14	L_max	5

Table 9 compares the accuracy of the best ensemble with the mean of all 17 models by age classes. The accuracy of the mean of the models was shown in figure 5. The table shows that the best ensemble improved the accuracy of prediction for all age classes, except 13-year-old's which had 0% accuracy. A distribution plot like figure 5 for the best ensemble can be found in appendix D as figure 16.

Table 9. Comparison of the mean of all the 17 models (mean) with a total accuracy of 72.7% and the best ensemble model (Best Ens.) with a total accuracy of 78.6%. In all age-groups, the ensemble improves on the mean-model accuracy except 13 year-old's.

Age	1	2	3	4	5	6	7	8	9	10	11	12	13
Mean	93.8	90.1	81.2	76.9	71.3	70.7	62.1	63.5	61.4	47.1	43.4	44.1	0
Best Ens.	95.1	93.2	84.6	80.0	78.9	78.9	65.6	76.6	69.6	52.6	61.5	50.0	0

Outliers

Figure 8 shows 6 images which had an error after rounding of more than 1 year. All the images with more than 1 year in prediction error are shown in table 10, with comments by an expert on the most common mispredictions in table 11.

Figure 8. Images with index 13, 71, 270, 342, 362 and 369 from the test-set was miss-predicted by between 25% and 100% of the models

We observed that there were some cod otoliths that were outliers to all models and on all exposures (e.g. otoliths 71, 342, 362, and 369), to a family of models and on all exposures (e.g. otoliths: 13, 423), to some models and on one exposure (E.g otolith 308), and to both family of models and on some exposures (E.g. otolith 320).

We also observed that the number of large outliers did not correlate with model performance like B5-min, and B6-mid which had 7 and 9 outliers, but the best accuracy. While B4-max with the lowest accuracy (70.9%) had the least number of large outliers with only 6 mispredictions.

Correlation of predictions and cluster analysis

The correlation of models on the test-set predictions given in figure 9 show that the models correlates a lot on outlier predictions. The correlation from all the predictions on the test set varied between 0.988 to 0.999, with the lowest correlation found between B5-min and Medium-min. The correlation was calculated using Pearson's correlation with Euclidean distance.

From figure 9 we saw that the EfficientNetV2 family was correlated from the red block in the lower right corner. The dendrogram of figure 10 shows hierarchical clustering (HCA) of the models. HCA found 3 clusters, b5-min, and B6-middle, which are the two best models, a cluster of all the EfficientNetV2 models, and a cluster of the rest of the models (figure 10).

Using K-Means together with the elbow- and silhouette-score-methods to find the optimal number of clusters, both found that there were 3 clusters in the correlation matrix (figure 11).

Figure 9. Pearson correlation of each model prediction on the test-set

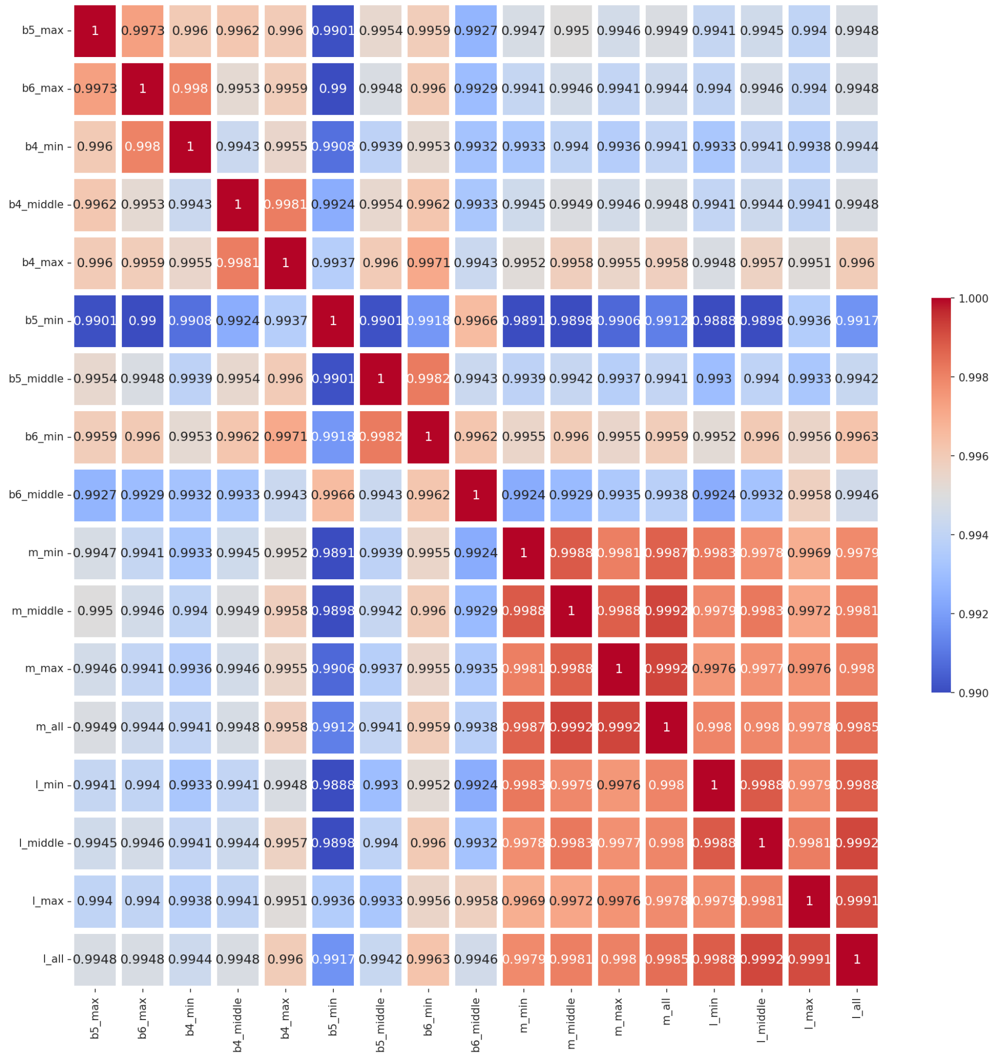

With K-Means and using 3 clusters we found similar clusters to HCA with the clusters:

- B5-max, and B6-max
- B4-min, B5-min, B6-min, B4-middle, B5-middle, B6-middle, B4-max
- EfficientNetV2 family of models

Figure 12 shows a scatter plot of two of the least correlated models, B5-min and Medium-min, which had Pearson's correlation 0.988. The red point inside the two circles is not a data point but "bullseye" if both models predict the correct age. The last sub-figure was the residual correlation of all age classes. It can be viewed in more

Figure 10. hierarchical clustering (HCA) on correlation of predictions

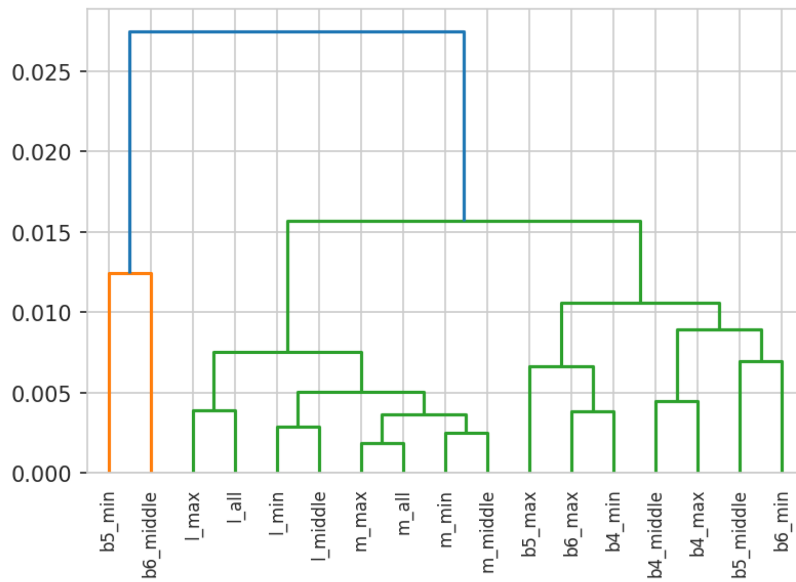

Figure 11. 1.Elbow method and 2. silhouette-score method

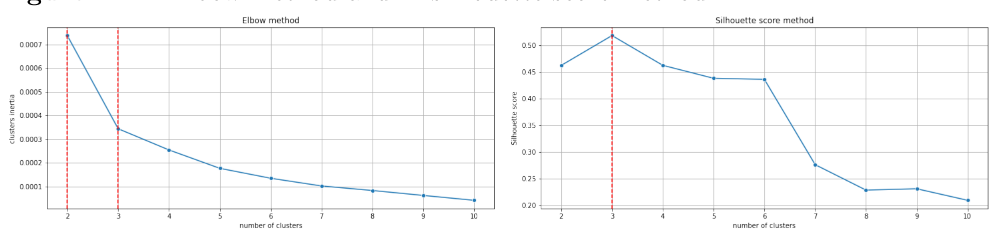

details in figure 13.

Discussion

During initial training, we trained a B4 network on ca 2000 images and obtained an accuracy of ca 60%, later another 3000 images were added and the same network was trained on ca 5000 images which resulted in accuracy of ca 70%. It could be interesting to investigate if adding another 3-5000 images would increase the accuracy to 80%.

To reach human level accuracy a score of 85% or higher is required ref-needed, and a score of 90% is considered good. Figure 14 shows a sample of 25 predictions on the validation-set during training.

Figure 12. Scatter plot of each age-class by Medium-min × B5-min.

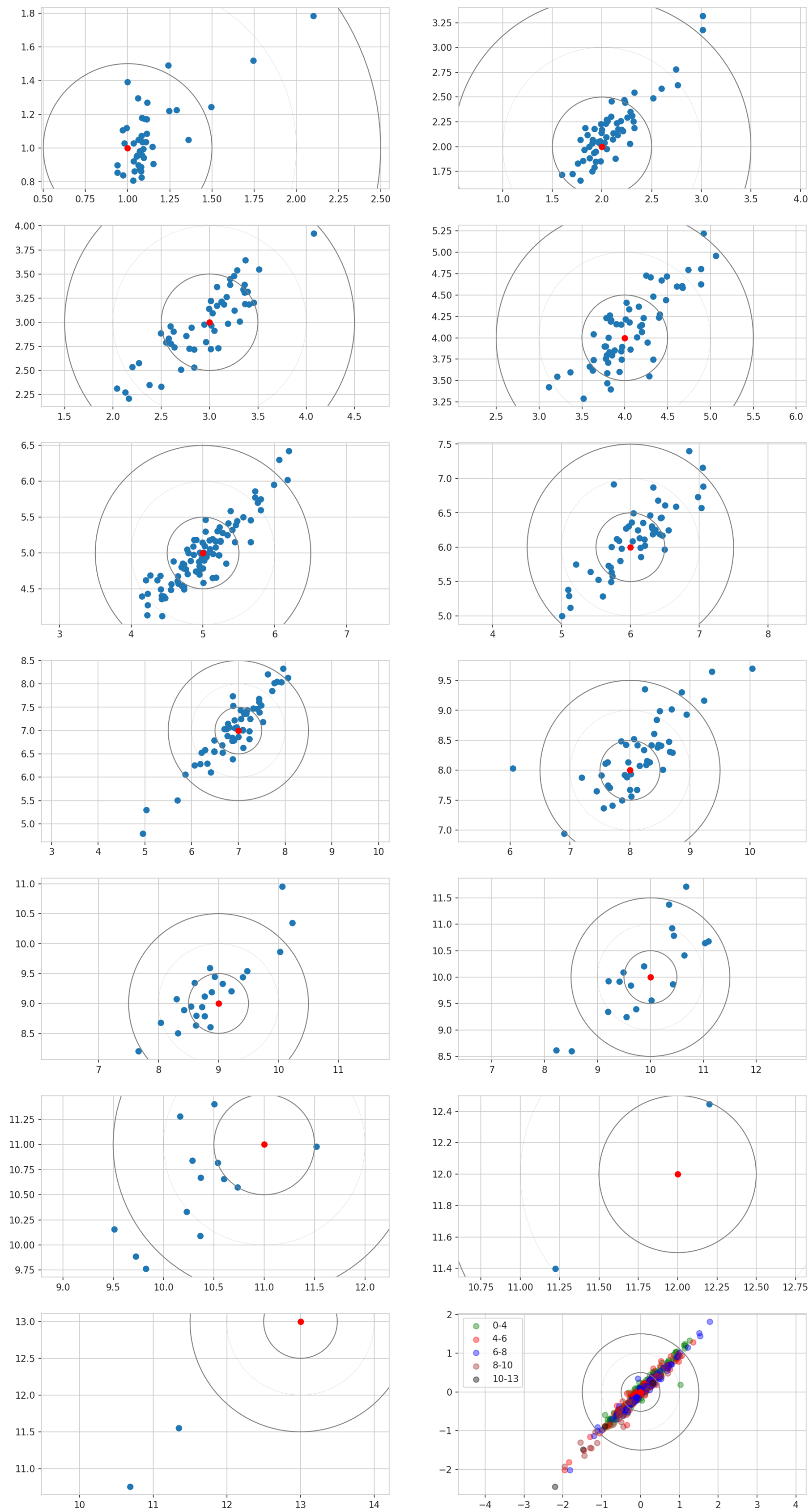

Figure 13. Scatter plot of the residuals of all age classes by Medium-min × B5-min.

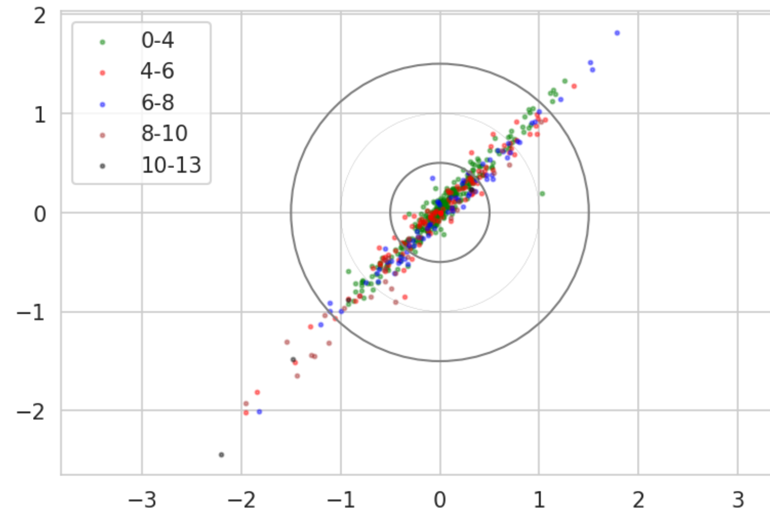

Figure 14. Sample of 25 predictions on a model of training on EfficientNetV2 size medium with minimum light exposure, left number is prediction, and right number is age read

The effect of data size

A crucial issue in machine learning projects is to determine how much training data is needed to achieve a specific performance goal. In computer vision, one commonly used rule of thumb adopted from the number of images and classes in the ImageNet dataset, is to have a thousand images for each class. In our case of cod otolith images the task entails regression towards 13 age classes instead of classification into 1000 classes. Therefore, approximately 13,000 images would appear to be the optimal number for our problem based on the rule of thumb for computer vision. This number can be reduced if transfer learning is applied for images within a similar domain. For cod otolith images, the domain is different than images in ImageNet. However, despite the different image domain for our problem we do see a significant performance boost in using transfer learning, suggesting that fewer images are needed than if trained from scratch. Excessive use of augmentation also reduces the number of images required. On the other hand, a general insight from deep learning is that more training data is always advantageous. Given the use of transfer learning and augmentation, the number of images used in this study, around 5000, might be close to the optimal, but we still think that a larger training set would improve performance. During initial training we trained a B4 network on about 2000 images and obtained an accuracy of around 60%. Later another 3000 images was added and the same network was trained on around 5000 images which resulted in accuracy of about 70%. This suggests to us that if our training set where even larger, say 10,000 images, this would boost performance further, maybe even approaching human level accuracy of 85%.

Accuracy for different age classes

All models tend to predict younger year classes with greater accuracy than older year classes. Pooling all models, prediction accuracy for 1–3 year old otoliths is ¿ 80%, exceeding 90% for one year old's. Accuracy tends to decline with increased age, especially for otoliths older than 9 years for which the training set is less represented than for younger otoliths (Figure 2). On the other hand, age 5 is the most abundantly represented age class in the training set, and accuracy for this age class is lower than the less abundant one-year-old age class. Thus, the CNN appears to be particularly competent at analyzing cod otoliths with fewer growth zones. ... Let us discuss why this is so... Ask the readers/biologists.

Ensemble of models

We should discuss the improved accuracy gained when combining models into ensemble of models (table 8). The best combinations show accuracy greater than 75%. Add a comment on the relation between variation in accuracy and the resulting accuracy of the ensemble (predictions of B4/5/6 have higher variance, but their ensembles win).

Moved from introduction to Discussion –

Accuracy, efficiency and cost benefits of CNN classifiers versus manual reading

. . . Despite fast progress the results remain mixed and often yield lower precision and consistency than those obtained by trained human readers, which limits the application of automated methods in real conditions. However, one aspect that is often under considered by such studies are the practical time and cost benefits that implementing a functional ML framework would provide. As noted by Fisher and Hunter (2018) (Fisher and Hunter, 2018) in their review of digital techniques for otolith analysis, "costs for human and machine ageing systems are broadly similar since a large part of the cost is associated with preparing the otolith sections". As such, the net benefit of automated ageing routines is directly dependent on the ability to scale performance using a comparatively smaller number of samples than human readers or, alternatively, to train them on "rougher" data that can be produced faster and at a more efficient cost. Also, CNN can be applied without high additional cost or even be incorporated in the routine protocols, but add a new value e.g., reading consistency check, time-drifts evaluations, inter-reader comparisons (how much 'off' is each reader when compared to the CNN predictions, even if not compared with the same otolith samples), etc.

We see the process of CNN implementation as an evolution of the protocols, with the intensive phase of model development and training. Gradual improvement of model reliability should then allow for the application of CNN as a complementary supportive tool for the age traditional estimations. Finally, this change should aim to scale the capacity of the age reading experts and improve sampling in the areas, fish stocks, or periods that lack proper reading effort.

Conclusion

Our results demonstrate that the use of deep learning techniques in the analysis of otoliths have a major potential for facilitating automation. We believe that carefully trained CNNs could become a major component in automated pipelines that require minimal processing and could be able to produce near at sea age estimates.

When developing the framework for the automatic age estimation, it is advised to include B4 architectures as they are quick to train, and performs good. Ensemble approaches are also recommended if more effort is favorable, as it gives a more robust and higher performing prediction. For a quick-to-train ensemble, B5 and Medium could be added. It is recommended to use under-exposed images.

References

References

Abadi, M., Agarwal, A., Barham, P., Brevdo, E., Chen, Z., Citro, C., Corrado, G. S., Davis, A., Dean, J., Devin, M., et al. (2016). Tensorflow: Large-scale machine learning on heterogeneous distributed systems. *arXiv preprint arXiv:1603.04467.*

Albuquerque, C. Q., Lopes, L. C. S., Jaureguizar, A. J., and Condini, M. V. (2019). The visual quality of annual growth increments in fish otoliths increases with latitude. *Fisheries Research, 220: 105351.*

Beamish, R. J. and McFarlane, G. A. (1995). A discussion of the importance of aging errors, and an application to walleye pollock: the world's largest fishery. in recent developments in fish otolith research. *University of South Carolina Press, Columbia, S.C., pp. 545–565.*

Brunel, T. and Piet, G. J. (2013). Is age structure a relevant criterion for the health of fish stocks? *ICES Journal of Marine Science, 70: 270–283.*

Campana, S. (2001). Accuracy, precision and quality control in age determination, including a review of the use and abuse of age validation methods. *Journal of fish biology*, 59(2):197–242.

Carbonara, P. and Follesa, M. C. (2019). Handbook on fish age determination: a mediterranean experience. *General Fisheries Commission for the Mediterranean. Studies and Reviews, 98: 1–179.*

Chollet, F. and others (2018). Keras 2.1.3. https://github.com/fchollet/keras.

et al., M., Thorsen, A., Godiksen, J., Malde, K., and Handegard, N. (2019). An efficient protocol and data set for automated otolith image analysis. *GeoScience Data Journal*.

Fisher, M. and Hunter, E. (2018). Digital imaging techniques in otolith data capture, analysis and interpretation. *Marine Ecology Progress Series, 598: 213–231.*

Francis, R. C. and Campana, S. E. (2011). Inferring age from otolith measurements: a review and a new approach. *Canadian Journal of Fisheries and Aquatic Sciences. NRC Research Press Ottawa, Canada. https://cdnsciencepub.com/doi/abs/10.1139/f04-063 (Accessed 3 February 2022).*

Hidalgo, M., Rouyer, T., Molinero, J. C., Massutí, E., Moranta, J., Guijarro, B., , and Stenseth, N. C. (2011). Synergistic effects of fishing-induced demographic changes and climate variation on fish population dynamics. *Marine Ecology Progress Series, 426: 1–12.*

Høie, H., Millner, R. S., McCully, S., Nedreaas, K. H., Pilling, G. M., and Skadal, J. (2009). Latitudinal differences in the timing of otolith growth: A comparison between the barents sea and southern north sea. *Fisheries Research, 96: 319–322.*

Krizhevsky, A., Sutskever, I., and Hinton, G. E. (2012). ImageNet Classification with Deep Convolutional Neural Networks. In Pereira, F., Burges, C. J. C., Bottou, L., and Weinberger, K. Q., editors, *Advances in Neural Information Processing Systems 25*, pages 1097–1105. Curran Associates, Inc.

LeCun, Y., Bengio, Y., and Hinton, G. (2015). Deep learning. *Nature*, 521(7553):436–444.

Loshchilov, I. and Hutter, F. (2016). Sgdr: Stochastic gradient descent with warm restarts. *neurips.*

Mahé, K. (2009). Project no. 044132. *Automated FISh Ageing (AFISA): final activity report.*

Mingxing Tan and, Q. V. L. (2021). Efficientnetv2: Smaller models and faster training. *CoRR*, abs/2104.00298.

Moen, E., Handegard, N. O., Allken, V., Albert, O. T., Harbitz, A., and Malde, K. (2018). Automatic interpretation of otoliths using deep learning. *Plos One.*

Panfili, J., de Pontual, H., Troadec, H., and Wrigh, P. J. (2002). Manual of fish sclerochronology. *https://archimer.ifremer.fr/doc/00017/12801/ (Accessed 3 February 2022).*

Paszke, A., Gross, S., Massa, F., Lerer, A., Bradbury, J., Chanan, G., Killeen, T., Lin, Z., Gimelshein, N., Antiga, L., Desmaison, A., Kopf, A., Yang, E., DeVito, Z., Raison, M., Tejani, A., Chilamkurthy, S., Steiner, B., Fang, L., Bai, J., and Chintala, S. (2019). Pytorch: An imperative style, high-performance deep learning library. In Wallach, H., Larochelle, H., Beygelzimer, A., d'Alché-Buc, F., Fox, E., and Garnett, R., editors, *Advances in Neural Information Processing Systems 32*, pages 8024–8035. Curran Associates, Inc.

Politikos, D. V., Petasis, G., Chatzispyrou, A., Mytilineou, C., and Anastasopoulou, A. (2021). Automating fish age estimation combining otolith images and deep learning: The role of multitask learning. *Fisheries Research, 242: 106033.*

Ragonese, S. (2018). Methuselah or butterfly? when fish age estimates and validations tell different stories. the case of the european hake (merluccius merluccius l. 1758) in the mediterranean sea. *"".*

Reglero, P. and Mosegaard, H. (2006). Onset of maturity and cohort composition at spawning of baltic sprat sprattus sprattus on the basis of otolith macrostructure analysis. *Journal of Fish Biology, 68: 1091–1106.*

Russakovsky, O., Deng, J., Su, H., Krause, J., Satheesh, S., Ma, S., Huang, Z., Karpathy, A., Khosla, A., Bernstein, M., Berg, A. C., and Fei-Fei, L. (2014). Imagenet large scale visual recognition challenge.

Siskey, M. R., Wilberg, M. J., Allman, R. J., Barnett, B. K., and Secor, D. H. (2016). Forty years of fishing: changes in age structure and stock mixing in northwestern atlantic bluefin tuna (thunnus thynnus) associated with size-selective and long-term exploitation. *ICES Journal of Marine Science, 73: 2518–2528.*

Szegedy, C., Vanhoucke, V., Ioffe, S., Shlens, J., and Wojna, Z. (2015). Rethinking the inception architecture for computer vision. *CoRR*, abs/1512.00567.

Tan, M. and Le, Q. V. (2019). Efficientnet: Rethinking model scaling for convolutional neural networks. *CoRR*, abs/1905.11946.

Tyler, A. V., Beamish, R. J., and McFarlane, G. A. (1989). Implications of age determination errors to yield estimates. *ICES Journal of Marine Science, 108: 27–35.*

Vabø, R., Moen, E., Smoliński, S., Åse Husebø, Handegard, N. O., and Malde, K. (2021). Automatic interpretation of salmon scales using deep learning. *Ecol. Inform. 63, 101322 (2021).*

Wightman, R. (2019). Pytorch image models. `https://github.com/rwightman/pytorch-image-models`.

Xu, B., Wang, N., Chen, T., and Li, M. (2015). Empirical evaluation of rectified activations in convolutional network. *CoRR*, abs/1505.00853.

A Prediction error of more than 1.5 year

Table 10. Predictions error with residual of more than 1.5 year per model per index in test-set

Idx	13	17	47	48	71	92	154	270	279	308	312	320	334	342	362	369	393	418	423	444	462	481	502	Count
B4-min	9.8				5.1			11.7	9.9			5.5		11.1	5.1	8.2								8
B4-mid	9.7				5.4				10.2			5.4	7.5	11.3	4.9	8.3	10.6	9.5						10
B4-max	9.6				5.0				10.4					11.3	5.0	8.2								6
B5-min	9.6				4.8			11.7	9.7					10.8	5.3					11.0				7
B5-mid	9.8				6.7	11.5		11.8	9.8					10.9	5.3	8.4				10.7				9
B5-max	9.8				4.5	11.5			9.6	7.7				10.6	5.1	8.3								8*
B6-min	9.7			7.6	5.1				9.7					10.7	5.2	7.9	10.8	10.7					9.4	9
B6-mid	9.6				5.1			11.5	9.7					10.8	5.2	8.3	10.8						9.4	9
B6-max	9.8				5.2					5.7				10.7	5.2	8.2	10.6				6.5		9.4	9**
m-min					5.0	11.3			10.0					10.7	5.0	8.2			6.0					7
m-mid					4.9	11.2			10.0					10.3	5.1	8.2								6
m-max			6.5		5.1	11.2	8.7		10.2					10.5	5.1	8.1			6.3					9
m-all					5.0	11.2			10.1					10.5	5.3	8.2			6.2			8.4		8
l-min					5.1	11.5			9.8		9.3			10.7	5.2	8.3			5.1					8
l-mid					5.0				9.8		9.4	5.5		10.6	5.2	8.1	10.5		6.0					9
l-max		9.5			5.1				9.9	3.6		5.4		10.8	5.1	8.2			5.9			8.4		10
l-all		9.3			5.0				9.8					10.8	5.2	8.0	10.5		6.2			8.5		9
Age	8	8	8	6	7	13	7	10	8	1	11	7	6	13	7	10	9	11	8	11	5	10	11	-
Count	9	2	1	1	17	7	1	4	16	3	2	2	1	17	17	17	6	2	7	2	1	3	3	141
As pct	53	12	6	6	100	41	6	24	94	18	12	12	6	100	100	100	35	12	41	12	6	18	18	-

Table 11. Comments on the most frequently miss predicted otolith images

Idx	Comment
13	Labeled 8 years, and read as 10 years by the B-models (EfficentNet). The quality of the exposures was good, but there was a lot of split rings in the middle.
71	Labeled 7 years, and read as 5 years by all models. The exposures was very bright on all three axis, and the dorsal axis had a break line, and the plane was out of focus.
279	Labeled as 8 years, and read as 10 years by almost all models except B6-max. The exposures was of good quality, but there was split rings in the middle.
308	Labeled as 1 year, and read as 8 years, 6 years and 4 years by B5-max, b6-max, and Large-max respectively. The exposures was of good quality and the predicted age is obviously wrong.
342	Labeled as 13 years, and read as 11 years by all models. The quality of the exposures was good. The inner section is dark on the ventral side, the distal side is light, and the dorsal side has a break line.
362	Labeled as 7 years, and read as 5 years by all models. This image is mislabeled. The otolith is obviously 5 years old.
369	Labeled as 10 years, and read as 8 years by all models except B5-min. The quality of the exposures was good, but it had split rings in the middle on bright exposures, and the contrast is strong.
393	Labeled as 9 years, and was read as 11 years by B4-middle, all B6 exposures and Large-middle and -all. The middle and min exposures was too dark. Max exposure was nice.
423	Labeled as 8 years, and read as 6 years by all the EfficentNetV2 models except Medium-middle. The quality of the images was bad. All the exposures was over-exposed.

B Model mean and standard deviation of residual test set prediction per age class

Figure 15. Model mean and standard deviation of residual test set prediction by age class

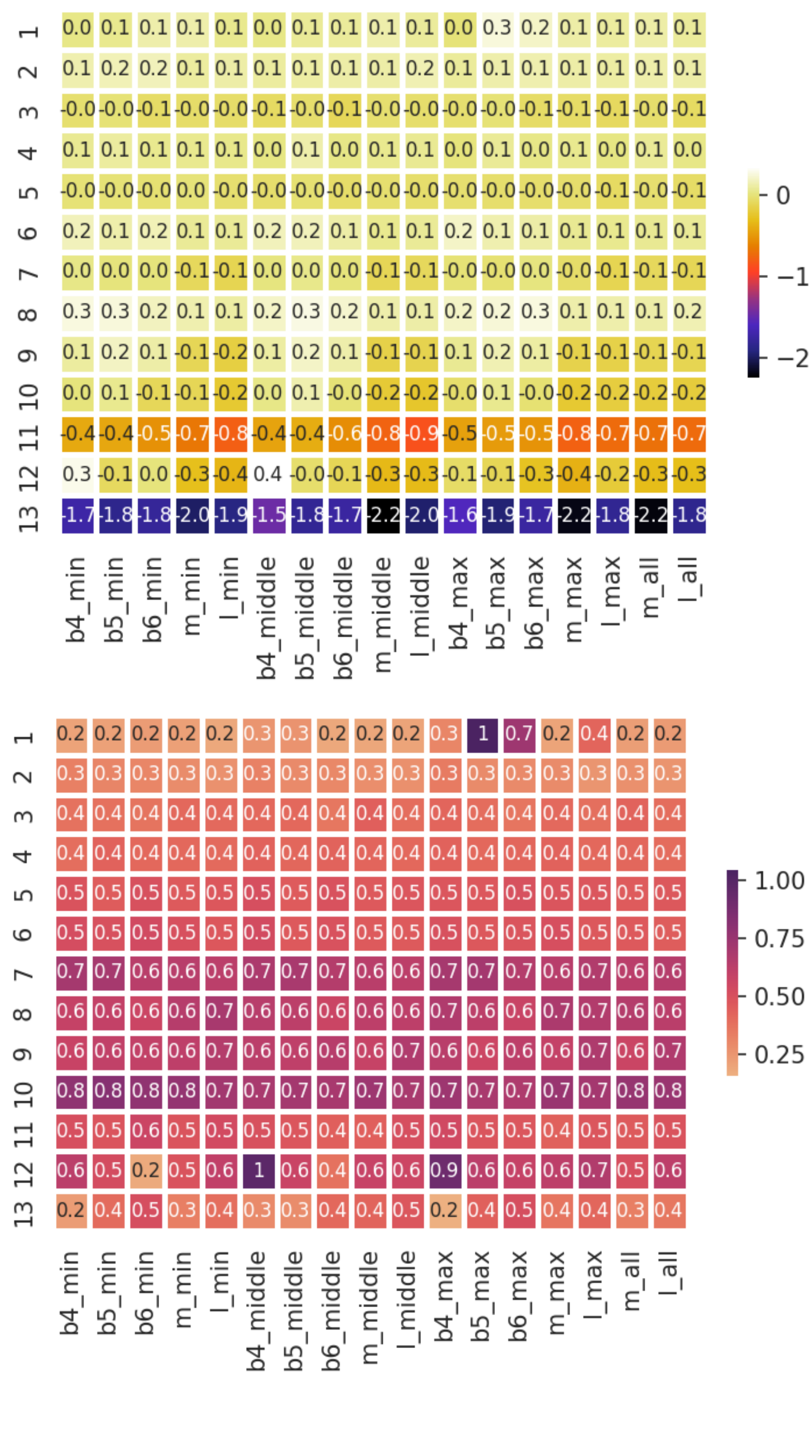

C Model accuracy and MSE per fold

Table 12. MSE per CNN per fold

CNN/fold	1	2	3	4	5	6	7	8	9	10	ens.	Mean
B4,min	.320	.318	.306	.313	.322	.314	.315	.316	.306	.302	.277	.313
B4,middle	.344	.328	.316	.334	.326	.320	.355	.326	.313	.325	.285	.329
B4,max	.340	.317	.318	.347	.336	.336	.336	.320	.354	.336	.291	.334
B5,min	.324	.322	.325	.336	.291	.314	.320	.331	.33	.317	.277	.321
B5,middle	.308	.286	.315	.349	.332	.310	.280	.275	.331	.288	.273	.307
B5,max	.472	.302	.437	.459	.432	.366	.356	.441	.438	.418	.359	.412
B6,min	.325	.329	.334	.293	.312	.290	.320	.300	.276	.306	.272	.309
B6,middle	.323	.301	.312	.268	.294	.266	.309	.311	.278	.289	.262	.295
B6,max	.435	.306	.306	.270	.390	.321	.411	.321	.294	.448	.305	.350
m,min	.292	.292	.294	.275	.298	.304	.304	.331	.307	.295	.273	.299
m,middle	.287	.302	.307	.332	.288	.276	.277	.294	.304	.278	.278	.295
m,max	.337	.297	.302	.291	.315	.347	.338	.321	.313	.283	.289	.314
m,all	.289	.299	.303	.284	.292	.287	.303	.288	.289	.294	.273	.293
l,min	.267	.316	.269	.270	.322	.332	.280	.307	.303	.299	.280	.297
l,middle	.300	.332	.320	.300	.272	.302	.294	.285	.307	.285	.275	.300
l,max	.322	.295	.324	.353	.295	.306	.271	.292	.380	.299	.286	.314
l,all	.285	.293	.283	.274	.286	.325	.272	.283	.277	.295	.271	.287
Mean	.328	.308	.316	.315	.318	.313	.314	.314	.318	.315	.284	.316

Table 13. Accuracy per CNN per fold

CNN/fold	1	2	3	4	5	6	7	8	9	10	ens.	Mean
B4, min	69.9	68.9	68.7	68.3	68.9	70.1	69.7	66.8	68.9	72.4	72.8	69.3
B4, middle	68.5	69.3	73.0	68.5	67.8	68.2	67.2	67.2	68.3	69.5	71.5	68.8
B4, max	64.1	68.2	67.2	66.2	67.8	69.5	67.2	69.3	66.2	65.2	70.9	67.1
B5, min	71.8	69.1	69.3	66.8	73.6	70.7	66.2	68.3	69.5	68.7	74.4	69.4
B5, middle	70.3	72.0	67.8	66.6	67.4	69.9	71.8	71.5	68.2	72.2	73.4	69.8
B5, max	71.3	71.1	67.4	73.2	66.4	68.9	64.1	69.1	68.7	71.8	73.2	69.2
B6, min	68.3	68.5	66.4	72.4	70.7	70.9	69.3	69.3	72.0	68.9	73.4	69.7
B6, middle	68.5	69.9	67.6	73.6	72.8	72.0	68.0	69.3	72.0	71.1	74.4	70.5
B6, max	70.5	68.2	65.2	73.2	69.1	67.8	68.0	68.0	72.8	68.5	71.5	69.1
m, min	71.1	71.1	69.5	73.4	71.8	70.9	70.9	69.7	70.1	71.5	74.0	71.0
m, middle	71.3	70.1	70.1	70.9	71.7	71.8	72.0	71.3	69.3	71.8	72.4	71.0
m, max	68.9	70.1	70.3	71.3	70.7	68.5	69.7	68.0	69.1	71.8	71.3	69.8
m, all	71.7	70.7	69.3	71.3	71.8	71.8	71.3	71.7	71.1	70.7	74.0	71.1
l, min	72.4	69.7	71.5	70.8	71.3	71.3	70.9	69.9	71.1	70.5	72.0	71.0
l, middle	68.7	68.0	69.7	71.8	71.1	71.1	69.7	70.5	71.1	72.0	72.8	70.4
l, max	71.1	70.1	69.9	74.2	72.8	71.1	72.2	71.1	71.1	70.1	72.4	71.4
l, all	71.8	71.7	71.8	71.7	71.7	68.0	73.2	71.7	73.0	71.5	72.2	71.6
Mean	70.0	69.8	69.1	70.8	70.4	70.1	69.5	69.6	70.1	70.5	72.7	70.0

477

D Prediction per age class using from best ensemble

Figure 16. Predictions by age class from the best ensemble.